Journal of the Ceramic Society of Japan 123 [5] 307-311 2015 Paper

Characterization of electronic structure around metal–insulator transition in $V_{1-x}W_xO_2$ thin films by thermopower measurement

Takayoshi KATASE, Kenji ENDO and Hiromichi OHTA†

Research Institute for Electronic Science, Hokkaido University, N20W10, Sapporo 001–0020, Japan

Electronic structure across the metal–insulator (MI) transition of electron-doped $V_{1-x}W_xO_2$ epitaxial films ($x = 0$–0.06) grown on α-Al_2O_3 substrates was studied by means of thermopower (S) measurements. Significant increase of $|S|$-values accompanied by MI transition was observed, and the transition temperatures of S (T_S) decreased with x in good linear relation with MI transition temperatures. $|S|$ values of $V_{1-x}W_xO_2$ films at $T > T_S$ were constant at low values of 23 $\mu V K^{-1}$ independently of x, which reflects a metallic electronic structure, whereas, those at $T < T_S$ almost linearly decreased with logarithmic W-concentrations. The gradient of $-213\ \mu V K^{-1}$ agrees well with $-k_B/e \cdot \ln 10$ ($-198\ \mu V K^{-1}$), suggesting that $V_{1-x}W_xO_2$ films have insulating electronic structures with a parabolic density of state around the conduction band bottom.

Key-words : Vanadium dioxide, Thermopower, Metal–insulator transition, Electronic structure

[Received November 26, 2014; Accepted December 28, 2014]

1. Introduction

Vanadium dioxide (VO_2) has attracted considerable attention due to its ability to reversibly transform from a low-temperature insulator into a high-temperature metal at ~340 K.[1] The metal–insulator (MI) transition is accompanied by a structural change from monoclinic to tetragonal-type rutile structure. The transformation of crystal structure originates from dimerization of vanadium ions with accompanying the position shifting from linear chains along c-axis of rutile phase to zigzag type, resulting in a monoclinic structure. The structural change causes reconstruction of electronic structures to open up a charge gap of ~0.6 eV that abruptly changes both the electrical resistivity and infrared transmission.[2] These features of the MI transition for VO_2 appear promising for potential applications to electrical and optical switching devices, operating at room temperature (RT). Recently, reversible alternation of electronic properties from insulator to metal state was demonstrated by both electrostatic charge-doping[3] and hydrogenation,[4] which enables on-demand-tunable devices using the MI transition of VO_2.

However, it still remains controversy on driving mechanism of the MI transition in VO_2, whether Peierls-type structurally-driven transition with electron–phonon interaction or Mott-type electrically-driven transition with electron-electron interaction.[5] Experimental investigation on the electronic-structure change across MI transition is necessary to elucidate its origin and should give crucial information for fundamental physics as well as for practical device application of VO_2. Thus, there have been many efforts to experimentally observe electronic structure mainly by spectroscopic techniques, such as X-ray photoemission spectroscopy (PES)[6] and angle resolved PES[7] for valence band structure observation, as well as X-ray absorption spectroscopy[8] for the conduction band structure, but the mechanism of the MI transition is not yet understood. Further investigation on the electronic-structure evolution by another experimental means is inevitable for the elucidation of MI transition of VO_2.

Here, we focused on thermopower (S) as a physical property to investigate the electronic structure across the MI transition. S-values should be sensitive to significant changes in the electronic structure of VO_2 at T_{MI} because S reflects the energy differential of density of state (DOS) around the Fermi energy (E_F), $[\partial \mathrm{DOS}(E)/\partial E]_{E=EF}$. In addition, the carrier concentration dependence of S-values for the insulating phase can clarify the shape of DOS at E_F due to the E_F shifts by carrier doping.[9] Although a few S measurements of undoped VO_2 have been reported,[10)–13)] there has been no report on electron-doped VO_2.

In this paper, we systematically investigated the S-values of electron-doped $V_{1-x}W_xO_2$ epitaxial films with different doping levels. Chemical substitution of VO_2 with aliovalent ions of W^{6+} is a classical way to effectively dope electrons[14] and reduce the T_{MI}.[15] Abrupt changes in the S-values accompanied by MI transition were observed for all the films and the transition temperature of S decreased with x in good linear relation with T_{MI}. We examined the electronic-structure changes of $V_{1-x}W_xO_2$ films across the MI transition by means of S measurements.

2. Experimental

$V_{1-x}W_xO_2$ epitaxial films were grown on $(11\bar{2}0)\alpha$-Al_2O_3 single-crystalline substrates by pulsed laser deposition. A KrF excimer laser (wavelength of 248 nm, laser energy fluence of 3 J cm^{-2}, and the repetition rate of 10 Hz) was used to ablate WO_3-added V_2O_5 polycrystalline target disks, which were prepared by sintering V_2O_5 and WO_3 powders mixed in a stoichiometric ratio of V_2O_5:$WO_3 = (1-x)/2$:x. The film composition of x was varied with the nominal composition of the targets. The growth temperature was fixed at 500°C and oxygen partial pressure (P_{O2}) was optimized at 2.0 Pa, because the ratio of resistivity change across MI transition is extremely sensitive to P_{O2} during thin film

† Corresponding author: H. Ohta; E-mail: hiromichi.ohta@es.hokudai.ac.jp

‡ Preface for this article: DOI http://dx.doi.org/10.2109/jcersj2.123.P5-1

DOI http://dx.doi.org/10.2109/jcersj2.123.307

growth.[16] After the deposition, the films were cooled to RT under the same oxygen pressure. The film thickness was fixed at ~20 nm, which was characterized by X-ray reflectivity measurement, and the deposition rate was ~2 nm min^{-1}.

3. Results and discussions

Figures 1(a) and 1(b) show out-of-plane (a) and in-plane (b) XRD patterns at RT for $V_{1-x}W_xO_2$ films with various doping levels ($x = 0$, 0.01, 0.022, 0.06). For out-of-plane XRD pattern **(a)** of an un-doped VO_2 film ($x = 0$), $h00$ ($h = 2$, 3, 4) diffraction peaks of monoclinic VO_2 (M) phase were observed along with intense peaks of α-Al_2O_3 substrate. The full width at the half maximum value of the out-of-plane rocking curve for 200 (M) was 0.2°. The in-plane XRD pattern **(b)** shows clear diffraction peaks of 020(M) and α-Al_2O_3 0006. The $2\theta_\chi$-fixed ϕ scan of the 020(M) diffraction in the inset shows a two-fold rotational symmetry with 180°, originating from the monoclinic symmetry of VO_2 lattice. These result substantiate that monoclinic VO_2 films were heteroepitaxially grown on α-Al_2O_3 substrates with the epitaxial relationship of (100)[010] $V_{1-x}W_xO_2$ (M) ∥ (11$\bar{2}$0)[0001]α-Al_2O_3. **Figures 2**(a) and 2(b) show topographic AFM image (a) and the schematic illustration of epitaxial growth model (b) for undoped VO_2 film on α-Al_2O_3 substrate. Many rectangular shaped grains were observed in the AFM image, which clearly reflects the anisotropic growth of VO_2 film along [1$\bar{1}$00] of α-Al_2O_3 substrate. As x increased in $V_{1-x}W_xO_2$ films, the peak intensity of 300 (M) weakened and disappeared at $x = 0.022$ [Fig. 1(a)]. Since the double lattice spacing along a-axis of monoclinic phase originates from the formation of vanadium-ion dimer, the disappearance of 300 (M) diffraction proves the transformation from monoclinic to rutile-type structure. For $V_{1-x}W_xO_2$ films with $x \geq 0.022$, $h0l$ ($h = l$) diffraction peaks of tetragonal VO_2 (T) were observed, indicating that the structural transition temperature decreased below RT. All obtained $V_{1-x}W_xO_2$ films with x up to 0.06 were confirmed to be epitaxially grown on α-Al_2O_3 substrates and the crystalline orientation kept unchanged, independently of x [Fig. 1(b)].

Temperature dependence of resistivity (ρ–T) and thermopower (S–T) was measured to investigate the MI transition characteristics of $V_{1-x}W_xO_2$ epitaxial films with $x = 0$–0.06, where the ρ–T and S–T were measured along [010](M) direction of $V_{1-x}W_xO_2$ films. ρ–T was measured by d.c. four probe method with van der Pauw electrode configuration. S–T was measured by giving a temperature difference of ~4 K in the film using two Peltier devices, where the actual temperatures of both sides of $V_{1-x}W_xO_2$ film surface were monitored by two tiny thermocouples [measurement setup for thermopower is shown in **Fig. 3**(a)]. The thermoelectromotive force (ΔV) and ΔT were simultaneously

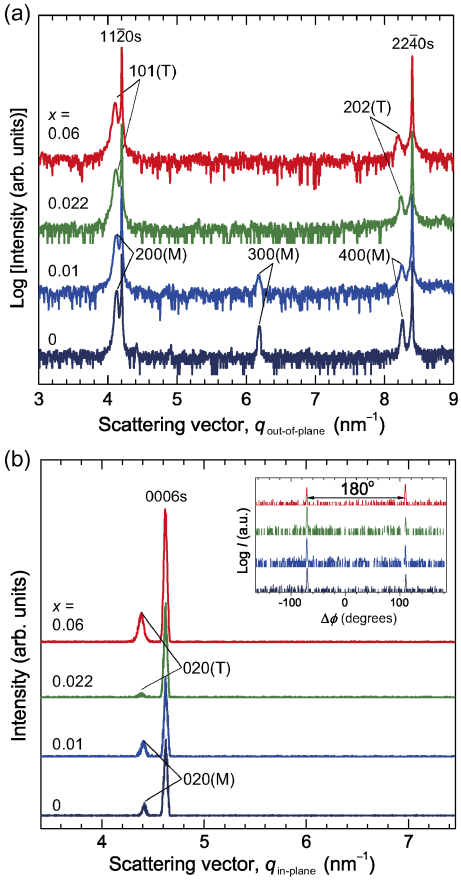

Fig. 1. Out-of-plane (a) and in-plane (b) XRD patterns at room temperature for $V_{1-x}W_xO_2$ epitaxial films with $x = 0$–0.06 grown on (11$\bar{2}$0)α-Al_2O_3 substrates. Crystalline phases and diffraction indices are noted above the corresponding diffraction peaks. M and T signify monoclinic and tetragonal structures, respectively. Inset of (b) shows in-plane ϕ scans of the diffraction peaks of $V_{1-x}W_xO_2$ films.

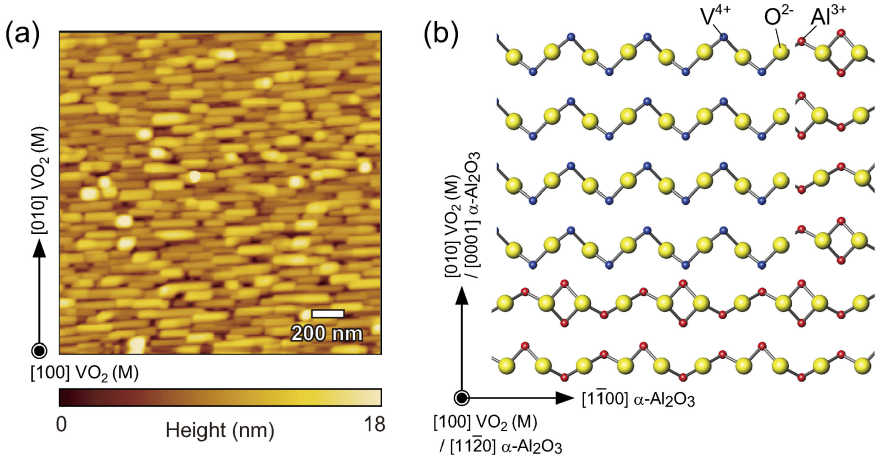

Fig. 2. (a) Topographic AFM image of VO_2 film ($x = 0$). (b) Schematic epitaxial relation of $V_{1-x}W_xO_2$/(11$\bar{2}$0)α-Al_2O_3. Many rectangular shaped grains were observed in AFM image, reflecting the anisotropic growth of VO_2 film along [1$\bar{1}$00] of α-Al_2O_3 substrate.

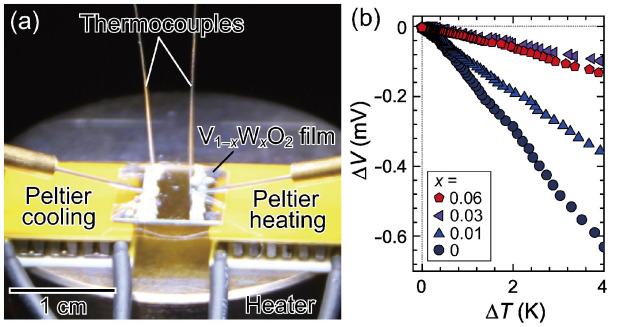

Fig. 3. (a) Photograph of thermopower measurement setup. The $V_{1-x}W_xO_2$ films were put on two Peltier devices, which give temperature gradient (ΔT) ~4 K in the film. The actual temperatures of both sides of $V_{1-x}W_xO_2$ film surface were monitored by two tiny thermocouples and thermo-electromotive force (ΔV) was simultaneously measured. (b) ΔV–ΔT plots at 300 K for $V_{1-x}W_xO_2$ epitaxial films with $x = 0$–0.06.

measured and the S-values were obtained from the slope of the ΔV–ΔT plots. ΔV–ΔT plots at 300 K for $V_{1-x}W_xO_2$ epitaxial films are shown in Fig. 3(b), which ensures a linear relationship between ΔV and ΔT.

Figure 4(a) shows ρ–T curves normalized by ρ at 350 K for $V_{1-x}W_xO_2$ epitaxial films with $x = 0$–0.06. Here, we normalized ρ to show the change of T_{MI} clearly, because ρ of $V_{1-x}W_xO_2$ epitaxial films were scattered even at the metallic state, where the average ρ was $3.1 \times 10^{-4}\,\Omega$cm with a standard deviation of $2.5 \times 10^{-4}\,\Omega$cm at 350 K. The average ρ was confirmed to be consistent with previously reported values of $V_{1-x}W_xO_2$ films.[15] The arrows indicate the position of T_{MI}, which is defined as the peak position of the derivative curve, $d[\log \rho]/dT$. The ρ of un-doped VO_2 film showed a sharp resistivity jump at T_{MI} of 338 K, which is similar to 341 K of VO_2 bulks.[1] Generally, epitaxial strains imposed on VO_2 films by substrates have a significant effect on T_{MI}. Compared to VO_2 films grown on (001) TiO_2 substrates,[17] where T_{MI} is depressed down to below 300 K without intentional doping, the VO_2 films on α-Al_2O_3 substrates are not subjected to an epitaxial strain effect, presumably because lattice relaxation of VO_2 occurs at the interface of the α-Al_2O_3 substrate due to the difference in crystallographic symmetry. With increase of x, the T_{MI} shifted to a lower temperature and became below RT at $x \geq 0.022$, which is consistent with the decrease in the structural transition temperature observed in the XRD measurements.

Figure 4(b) summarizes the S–T curves. The obtained S-values were negative in the entire temperature range, indicating that n-type carriers are dominant in both the metal and insulating phases of $V_{1-x}W_xO_2$ films. As the temperature decreases, significant increase and the saturation of S-values were observed for all films. It should be noted that it was hard to measure S-values of undoped VO_2 films at low temperature because of the high contact resistance >1 MΩ, i.e. reliable thermoelectromotive force was not obtained at low temperature. The saturated $|S|$-values of $V_{1-x}W_xO_2$ films ($x = 0.01$–0.06) decreased linearly with decrease of temperature down to zero, which is consistent with the linear decrease of S–T for insulating phase of undoped VO_2 bulk,[11] and suggesting that they are degenerate semiconductors. The transition temperatures (T_S), where S-values start to increase, are indexed by arrows. We compare the x dependences of T_S and T_{MI} (**Fig. 5**) extracted from ρ–T [Fig. 4(a)] and S–T [Fig. 4(b)]. T_S and T_{MI} were observed at almost the same temperature and monotonically decreased with an increase of x, which clearly

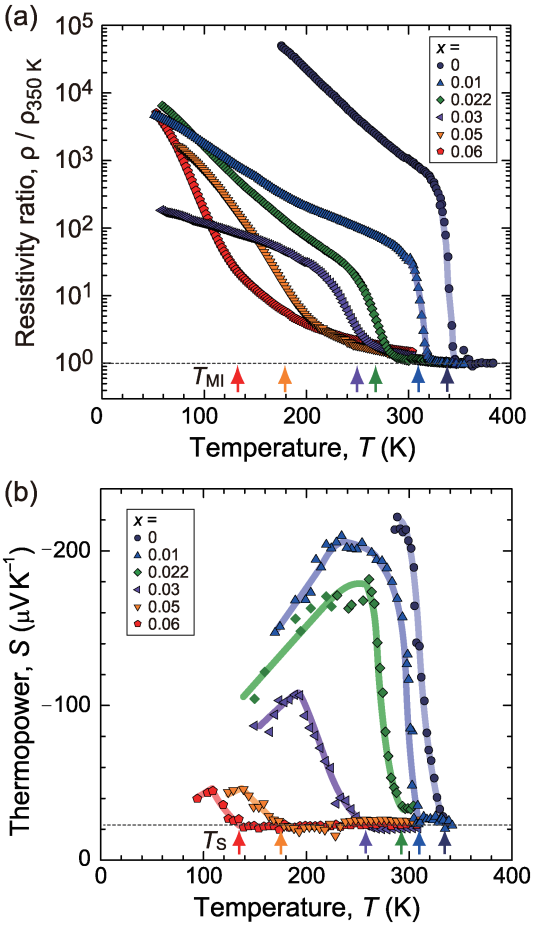

Fig. 4. Temperature dependences of the electrical resistivity (ρ) and the thermopower (S) of $V_{1-x}W_xO_2$ epitaxial films with $x = 0$–0.06. (a) ρ–T curves normalized by ρ at 350 K, ρ/ρ_{350K}. Transition temperatures of T_{MI}, indicated by arrows, gradually decrease as x increases. (b) S–T curves. Arrows denote the transition temperatures (T_S), where S-values start to increase.

indicate that the transition observed in S–T originates from electronic structure reconstruction at T_{MI}.

For metallic phase at $T > T_S$, the S-values of $V_{1-x}W_xO_2$ films were constant at $-23\,\mu V\,K^{-1}$ regardless of x [Fig. 4(b)], which agrees well with the previously reported S-values of $\sim -20\,\mu V\,K^{-1}$ for the metallic phase of un-doped VO_2 bulks,[10),11)] microbeams,[12)] and films.[13)] On the other hand, for the insulating phase at $T < T_S$, the saturated maximum $|S|$-values ($|S_{max}|$), which are defined as the $|S|$-values for intrinsic insulating phases,[11)] steeply decreased from $205\,\mu V\,K^{-1}$ ($x = 0.01$) to $43\,\mu V\,K^{-1}$ as x increased up to 0.06 [Fig. 4(b)]. $|S|$-values of insulating $V_{1-x}W_xO_2$ at low temperature showed T-linear tendency, suggesting that the $|S|$-value obeys Mott formula,

$$S = \frac{\pi^2}{3}\frac{k_B^2\,T}{e}\left\{\frac{d[\ln(\sigma(E))]}{dE}\right\}_{E=EF},$$

where $\sigma(E)$ is energy-dependent conductivity and k_B is Boltzmann's constant.[18] The Mott formula is most frequently used to explain S-values of metal and degenerate semiconductor, where the $|S|$-values decrease linearly with T by reflecting the gradient of DOS around E_F. Therefore, we used Mott formula divided by T, $|S_{max}|/T_{max}$, to compare the $|S_{max}|$-values of insulating $V_{1-x}W_xO_2$ films with different x at the same temperature. As

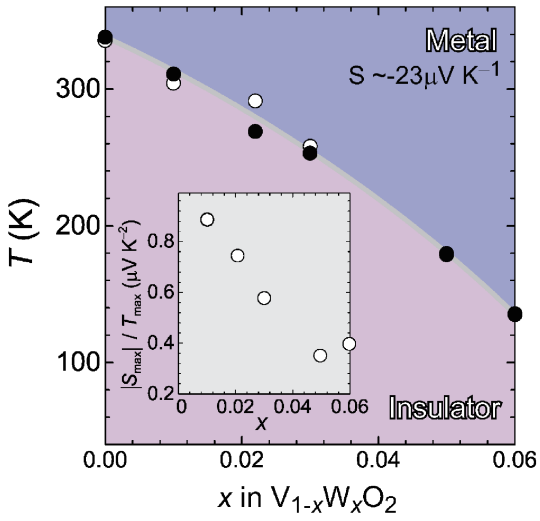

Fig. 5. x dependences of the transition temperatures of T_{MI} and T_s, which are extracted from ρ–T and S–T curves in Figs. 4(a) and 4(b), respectively. Closed and open symbols represent T_{MI} and T_s, respectively. For the metallic phase (upper part), S-values of $V_{1-x}W_xO_2$ films remain constant at $-23\,\mu V\,K^{-1}$ and independent of x. Inset figure shows x dependence of $|S_{max}|$ divided by T_{max}, which corresponds to

$$\frac{\pi^2}{3}\frac{k_B^2}{e}\left\{\frac{d[\ln(\sigma(E))]}{dE}\right\}_{E=EF}.$$

The $|S_{max}|/T_{max}$ value decreases with an increase of x.

shown in the inset of Fig. 5, $|S_{max}|/T_{max}$ monotonically decreased with increasing x, suggesting that the $[\partial DOS(E)/\partial E]_{E=EF}$ becomes moderate with an increase of x.

In order to construct the carrier density (n_e) dependence of S-values for the $V_{1-x}W_xO_2$ films, Hall effect measurement with van der Pauw electrode configuration was performed at RT, but reliable Hall voltages were not obtained, presumably due to the low carrier mobility ($\leq 0.1\,cm^2\,V^{-1}\,s^{-1}$) and high carrier concentration of the $V_{1-x}W_xO_2$ films.[19] Therefore, we used the W-concentration instead of n_e from doping levels (x) in $V_{1-x}W_xO_2$ films and plotted $|S_{max}|$ at 300 K [**Fig. 6**(a)]. In general, semiconductors possessing a parabolic DOS show a linear relationship between $|S|$ and the log of carrier density (log n_e):[20] $|S| = -k_B/e\cdot\ln 10$ (log $n_e + C$), where C is parameter that depend on the types of materials. $|S_{max}|_{300K}$ almost linearly decreased from 266 down to $105\,\mu V\,K^{-1}$ as a function of log [W] with a gradient of $-213\,\mu V\,K^{-1}$ decade^{-1}, which agrees well with $-k_B/e\cdot\ln 10$ ($= -198\,\mu V\,K^{-1}$ decade^{-1}). The linear decrease of S against log [W] suggests that S-values of $V_{1-x}W_xO_2$ films at $T < T_s$ reflects insulating electronic structures with a parabolic DOS around the conduction band bottom in the doping range of $x = 0.01$–0.06, which is consistent with the calculated band structure of insulating VO_2.[21]

Here, we summarize the present results, comparing with the suggested electronic structure of VO_2.[2] In principal, lower-energy t_{2g} state of the V 3d orbital splits into $d_{\parallel}$ band and π^* band. In the metallic T-phase, $d_{\parallel}$ band overlaps the π^* band, and E_F is located at the partially filled hybridized-band between the $d_{\parallel}$ and π^* states. This scenario is consistent with the constant S-values of $-23\,\mu V\,K^{-1}$ for $V_{1-x}W_xO_2$ films at $T > T_{MI}$, independently of W-concentration [Fig. 6(a)]. In the insulating M-phase, dimerization of V ions raises the π^* band above E_F and the $d_{\parallel}$ band splits into bonding- and antibonding-$d_{\parallel}$ states,

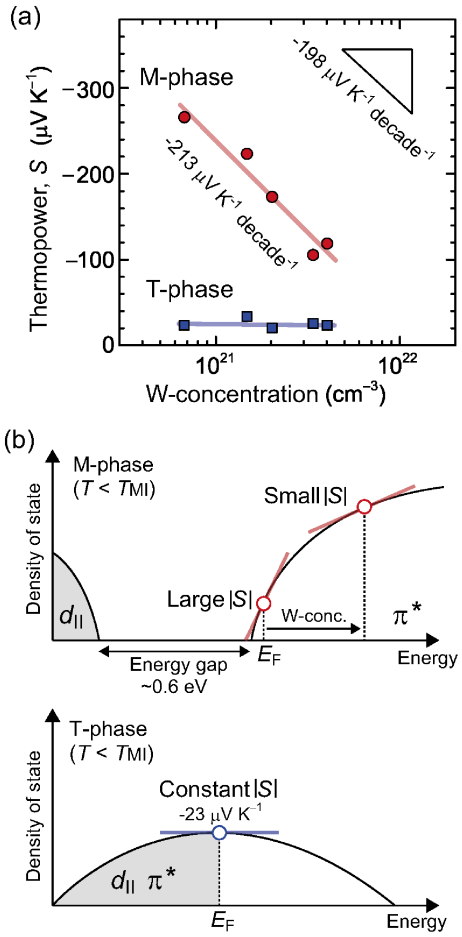

Fig. 6. Thermopower analysis of the electronic structure for metallic T-phase ($T > T_{MI}$) and insulating M-phase ($T < T_{MI}$) of $V_{1-x}W_xO_2$ films. (a) Relationship between $|S|$ at 300 K and W-concentration. For $|S_{max}|$ values of M-phase, gradient of $-213\,\mu V\,K^{-1}$ decade^{-1} agrees well with $-k_B/e\cdot\ln 10$ ($= -198\,\mu V\,K^{-1}$ decade^{-1}). (b) Schematic electronic structure of T-phase (lower) and M-phase (upper) for $V_{1-x}W_xO_2$ around E_F. In case of M-phase, E_F shifts to the higher energy side by W-doping in the empty π^* band possessing a parabolic DOS.

creating a charge gap between π^* band and antibonding-$d_{\parallel}$ band. Therefore, the steep decrease in the $|S_{max}|$-values with x and the linear relation of $|S_{max}|$ against log [W], observed in $V_{1-x}W_xO_2$ films at $T < T_{MI}$, indicate that the doped carriers are simply accomodated in the π^* band possessing a parabolic DOS in the doping rage of $x = 0.01$–0.06, as illustrated in Fig. 6(b).

4. Summary

In summary, we investigated the S-values of electron-doped $V_{1-x}W_xO_2$ epitaxial films grown on α-Al_2O_3 substrates to experimentally examine the electronic-structure change across the MI transition. $|S|$ values of $V_{1-x}W_xO_2$ films at $T > T_S$ were independent of x and remain constant at low values of $23\,\mu V\,K^{-1}$, which reflects the metallic electronic structure. On the other hand, those at $T < T_S$ almost linearly decreased with logarithmic W-concentrations. The gradient of $-213\,\mu V\,K^{-1}$ agrees well with $-k_B/e\cdot\ln 10$ ($-198\,\mu V\,K^{-1}$), suggesting that they have insulating electronic structures with a parabolic density of state around the conduction band bottom in the doping range of $x = 0.01$–0.06. The present results should provide crucial information not only for fundamental physics but also for practical device applications of VO_2.

Acknowledgments This work was supported by Grant-in-Aid for Scientific Research A (No. 25246023), Grant-in-Aid for Scientific Research on Innovative Areas (No. 25106007) from the Japan Society for the Promotion of Science (JSPS), and partly supported by the Asahi Glass and Murata Science Foundation.

References

1) F. J. Morin, *Phys. Rev. Lett.*, 3, 34–36 (1959).
2) J. B. Goodenough, *J. Solid State Chem.*, 3, 26–38 (1971).
3) M. Nakano, K. Shibuya, D. Okuyama, T. Harano, S. Ono, M. Kawasaki, Y. Iwasa and Y. Tokura, *Nature*, 487, 459–462 (2012).
4) J. Wei, H. Ji, W. Guo, A. H. Nevidomskyy and D. Natelson, *Nat. Nanotechnol.*, 7, 357–362 (2012).
5) R. M. Wentzcovitch, W. W. Schulz and P. B. Allen, *Phys. Rev. Lett.*, 72, 3389–3392 (1994); A. Zylbersztejn and N. F. Mott, *Phys. Rev. B*, 11, 4383–4395 (1975).
6) E. Sakai, K. Yoshimatsu, K. Shibuya, H. Kumigashira, E. Ikenaga, M. Kawasaki, Y. Tokura and M. Oshima, *Phys. Rev. B*, 84, 195132 (2011).
7) K. Saeki, T. Wakita, Y. Muraoka, M. Hirai, T. Yokoya, R. Eguchi and S. Shin, *Phys. Rev. B*, 80, 125406 (2009).
8) M. Abbate, F. M. F. de Groot, J. C. Fuggle, Y. J. Ma, C. T. Chen, F. Sette, A. Fujimori, Y. Ueda and K. Kosuge, *Phys. Rev. B*, 43, 7263–7266 (1991).
9) H. Ohta, Y. Masuoka, R. Asahi, T. Kato, Y. Ikuhara, K. Nomura and H. Hosono, *Appl. Phys. Lett.*, 95, 113505 (2009); Y. Nagao, A. Yoshikawa, K. Koumoto, T. Kato, Y. Ikuhara and H. Ohta, *Appl. Phys. Lett.*, 97, 172112 (2010).
10) C. N. Berglund and H. J. Guggenheim, *Phys. Rev.*, 185, 1022–1033 (1969).
11) C. Wu, F. Feng, J. Feng, J. Dai, L. Peng, J. Zhao, J. Yang, C. Si, Z. Wu and Y. Xie, *J. Am. Chem. Soc.*, 133, 13798–13801 (2011).
12) J. Cao, W. Fan, H. Zheng and J. Wu, *Nano Lett.*, 9, 4001–4006 (2009).
13) D. Fu, K. Liu, T. Tao, K. Lo, C. Cheng, B. Liu, R. Zhang, H. A. Bechtel and J. Wu, *J. Appl. Phys.*, 113, 043707 (2013).
14) C. Tang, P. Georgopoulos, M. E. Fine, J. B. Cohen, M. Nygren, G. S. Knapp and A. Aldred, *Phys. Rev. B*, 31, 1000–1011 (1985).
15) K. Shibuya, M. Kawasaki and Y. Tokura, *Appl. Phys. Lett.*, 96, 022102 (2010).
16) H. Kim, N. Charipar, M. Osofsky, S. B. Qadri and A. Piqué, *Appl. Phys. Lett.*, 104, 081913 (2014).
17) Y. Muraoka and Z. Hiroi, *Appl. Phys. Lett.*, 80, 583–585 (2002).
18) M. Jonson and G. D. Mahan, *Phys. Rev. B*, 21, 4223–4229 (1980).
19) D. Ruzmetov, D. Heiman, B. B. Claflin, V. Narayanamurti and S. Ramanathan, *Phys. Rev. B*, 79, 153107 (2009).
20) G. H. Jonker, *Philips Res. Rep.*, 23, 131 (1968).
21) E. Caruthers and L. Kleinman, *Phys. Rev. B*, 7, 3760–3766 (1973).